

Balloon Payload Automated Recovery System (B-PARS)

William B. Valentine¹, Zachary T. Murdock², Spencer H. Lueckenotto³
Wichita State University, Wichita, Kansas 67260-0044

This report contains the investigation and development of a reusable system to carry instruments to high altitudes by use of a balloon and then reliably return them to a selected landing site. A fixed wing glider was selected to carry out the return portion of the mission. Tests were carried out to verify the performance of the vehicle and the reliability of an autonomous system to execute the desired mission.

Nomenclature

CNC	= Computer Numerical Control
APRS	= Automated Packet Reporting System
AH	= Amp Hour
WH	= Watt Hour
W	= Watt
V	= Volt
A	= Ampere
L	= Lift
D	= Drag
AOA	= Angle of attack
Lat	= Latitude
Lng	= Longitude
Alt	= Altitude
VX	= Horizontal ground velocity
VZ	= Vertical Velocity
Q	= Dynamic Pressure

I. Introduction

High altitude balloons are used regularly to carry devices called radiosondes which collect data about conditions in the upper atmosphere. The National Weather Service (NWS) launches around 184 of these a day across the US, however only about 20% of them ever get returned. More precise instruments can also be carried by high altitude balloons, and sometimes even cubesats. These payloads pose a large financial risk though because of the high chance that the payload will be lost, especially if launching near large bodies of water or difficult terrain.

The goal of this project is to autonomously return a payload from a high-altitude balloon to the launch point, or to an otherwise decided safe landing location where a recovery can be made. The return would be done with a plane that is around two pounds in weight and is fully autonomous plane. It would then be able to keep expensive equipment from being lost and would reduce the amount of lost “cheap” radiosondes. Both improvements would further the research opportunities in Earth’s high atmosphere. This model is however, a proof of concept; due to its small two-pound size, it is not capable of carrying much additional weight, but it is instead designed to demonstrate that a larger model (approximately twice as big) could be made and would have approximately a 2 pound payload weight. Background

¹ Student, Aerospace Engineering, and AIAA Member Grade for first author.

² Student, Aerospace Engineering, and AIAA Member Grade for first author.

³ Student, Aerospace Engineering, and AIAA Member Grade for first author.

A. Previous Related Projects

A couple of similar projects assisted B-PARS in its successes and development, namely Buerge Engineering Corporation's Courier projects and the High-Altitude Balloon Launched Experimental Glider (HABLEG) developed by the Robotics and Mechatronics Center, German Aerospace Center (DLR). Both projects had their successes and shortcomings which B-PARS considered during design and development.



Figure 1. HABLEG Project



Figure 2. BEC's Courier Line

In the project put on by Buerge Engineering Corporation (BEC), the mission was very similar: to be able to return a payload dropped from a weather balloon at 100,000 feet to the original landing site [2]. The design of the aircraft included a flying wing design with about a 36-inch wingspan. The model was made from insulation foam, much like the foam we have available to us as students at Wichita State. BEC took iterative approaches to their vehicle solution. In the end, they created over five iterations of their "Courier" product line as shown in Figure 2. Many things were learned from this, including that low aspect ratio wings give better structural stability, low aspect ratio wings have decreased glide performance, flutter is a common issue with control surface on high-altitude vehicles travelling at high speeds, and thermal resistance is key for electronics, as temperatures fall below -30 degrees Fahrenheit as the altitude rises. Most consumer electronic equipment is built for temperatures above this threshold.

In another project examined by the Robotics and Mechatronics Center, German Aerospace Center (DLR), we found a similar mission, but a different platform than the one used by BEC. The DLR vehicle named HABLEG (High-Altitude Balloon Launched Experimental Glider) was a larger scale model at a three-meter wingspan, which is larger than BEC's vehicle, and much larger than B-PARS [1]. The HABLEG shown in Figure 1 possesses an interesting aspect which is becoming more commonly available to typical consumers at a lower price: a long-range telemetry and video feed. This system allowed the HABLEG to receive commands from a manned ground station in flight, and the whereabouts, altitude, flight speed and other important telemetry data was accessible at every second of the approximately 145-minute mission. The size of the HABLEG allows it to more easily fit the necessary power and electronic equipment onboard, so the benefits of having this capability did not justify its place amongst the necessary components in B-PARS, such as flight control systems, servos and the parachute mechanism. This telemetry system would have added weight as well as nearly tripled B-PARS' power capacity necessary to complete the mission.

HABLEG did find that during the transition period from vertical to horizontal flight oscillations were occurring to the vehicle, and if it were not for the manual telemetry inputs from the trained ground crew, the mission may have been a failure. This was neither confirmed or denied in the report, but due to technology advances in autopilot and hobby-grade flight systems, this telemetry link was deemed unnecessary for this mission. In the end, the HABLEG was a successful demonstration of a high-altitude balloon launched glider, so this proves the feasibility of the proposed mission.

B. Mission Legality

By using a communication link and other components to control the descent of the payload, the vehicle is almost certainly considered a small unmanned aircraft system (small UAS) as defined in 14 CFR 107.03 [4]. With that said, 14 CFR 107.1 [4] lists various ways one can be exempt from the rules associated with it:

"§ 107.1 Applicability. (a) Except as provided in paragraph (b) of this section, this part applies to the registration, airman certification, and operation of civil small unmanned aircraft systems within the United States. (b) This part does not apply to the following: (1) Air carrier operations; (2) Any aircraft subject to the

provisions of part 101 of this chapter; or (3) Any operation that a remote pilot in command elects to conduct pursuant to an exemption issued under section 333 of Public Law 112–95, unless otherwise specified in the exemption.”

Title 14 Part 101 Subpart D sections 31 through 43 (14 CFR 101.31-43) [4] detail the unmanned free balloon exemption which will allow the vehicle to be legal despite being a UAS. The exemption contains no sections with which the plane does not comply. Specifically, all equipment requirements listed in 14 CFR 101.35 [4] are met. As the operators, we can provide forecasts ahead of time to the ATC of the trajectory of balloon ascent and payload descent (estimated time and location) as requested by 14 CFR 101.37 [4], and can provide the required positional updates in two hour periods during the launch as stipulated in 14 CFR 101.39 [4]. Only once in the entire subpart (14 CFR 101.31-43) [4]. is the descent mention, stating only that operators report the estimated time and location before and during the launch (14 CFR 101.37-39) [4]. Suspension devices (such as parachutes) are mentioned once in the subpart (14 CFR 101.35) [4], and only in a provision about using a suspension device longer than 50 feet during the night. With all of that in mind, a reasonable argument is made that an unpowered (i.e. no propulsion system) method of controlled descent has no reason to not fall under the exemptions of Title 14 part 101 subpart D [4].

II. Experimental Approach

C. Mission Return Calculations

An excel sheet was created to simulate and predict vehicle glide distance while accounting for high altitude winds. Winds from a sounding balloon could be fed into the program, which would then predict the path that the balloon would follow on the ascent, as well as predict the potential glide distance available from an input drop altitude. The data shown is from a prediction ran from winds recorded by a sounding balloon released in Topeka, Kansas on a particularly windy day. The mission prediction calculator in Excel was initially used to size our wing as well as give an idea of required L/D to reliably make a return to launch site flight. It was desired to obtain a return to launch site safety factor of 1.5, meaning that even with winds accounted for, our vehicle could glide 1.5 times the distance needed to return to the launch site. It was determined that to meet this safety factor with a reasonable L/D of 5, a small wing area, high wing loading configuration was needed. This resulted in a much higher glide speed, making a return to launch site much more practical, but made low altitude testing much more difficult. To mitigate some of the risks of such a high glide speed at low altitude, the decision was made to include a parachute on the vehicle, which will be discussed in more detail later on. As can be seen (Table 1), the current vehicle configuration is predicted to achieve a return to launch safety factor of 1.6 for this particular sounding data. The winds are typically strongest in the zone from 20,000- 40,000 feet, and so the majority of the return flight must occur above these altitudes. For this simulation, the vehicle returns to the launch site at roughly 55,000 feet (Figure 3) and will loiter (fly in a circular path) until it reaches a low enough altitude for the parachute to deploy. Figure 4 shows the projected ground track for both the balloon ascent phase and gliding phase. The gliding phase estimation assumes a straight line is flown all the way until the ground to get an estimation for total glide distance. In the actual mission, once the vehicle is over the desired landing site it will switch modes and circle until it descends low enough for the parachute to deploy.

CL/CD Max	5.00
CL	0.20
CD	0.04
Drop Altitude	100000.00 ft
Range (no wind)	94.70 miles
Weight	2.00 lbf
Glide Angle	11.31 degrees
Wing Area	0.81 ft^2
Ascent Time	78.17 minutes
Glide Time	37.56 minutes
Total Mission Time	1.93 hours
Range (with wind)	66.97 miles
Glide Range Needed	41.86 miles
Excess Range	25.12 miles
Cruise Dynamic Pressure	12.65 psf
Sea Level Airspeed	101.15 ft/s
Max Airspeed	920.59 ft/s
Mach # at Drop Altitude	0.93
Average True Airspeed:	239.80 ft/s
Safety Factor:	1.60

Table 1. Engineering Mission Predictions

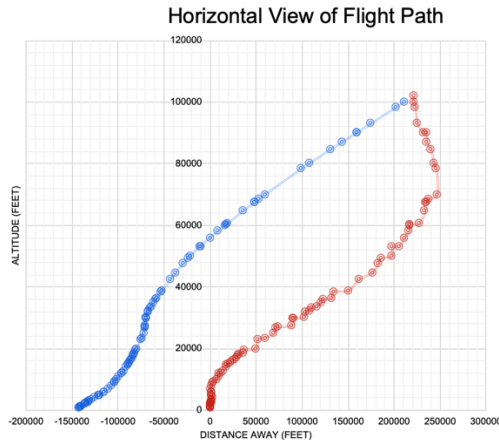


Figure 3. Horizontal Flight Path

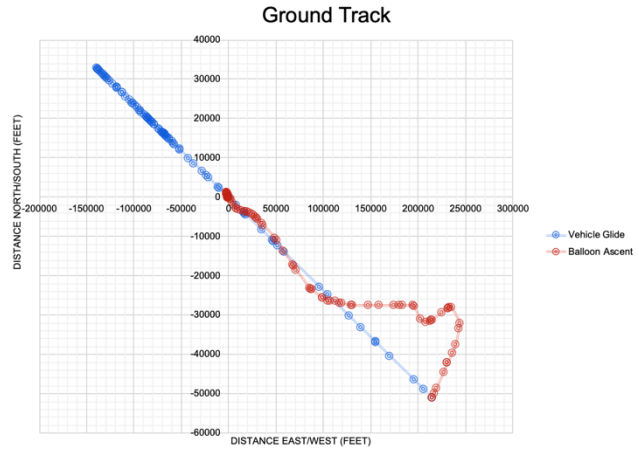


Figure 4. Predicted Ground Track

D. Performance Analysis in Open VSP

Open VSP is an open source software developed by NASA to model vehicle geometry (Figure 6) and perform estimations of performance. Open VSP was utilized in this project to perform initial conceptual design of the plane and to optimize appropriate tip twist and wing sweep to produce a stable configuration (Figure 5). The elevons were also analyzed in open VSP to get an estimation of max alpha trim. Open VSP assumes inviscid flow and does not account for skin friction drag. To help account for viscous effects the drag predictions output from Open VSP were tripled before being used to estimate L/D max. The performance estimates generated by Open VSP (Figure 5, 7) were fed into the mission prediction calculator in Excel and adjusted until a stable design capable of meeting mission requirements was obtained.

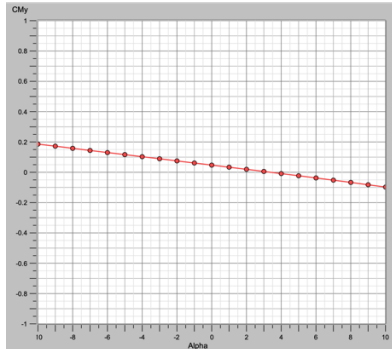


Figure 5. VSP Moment Polar

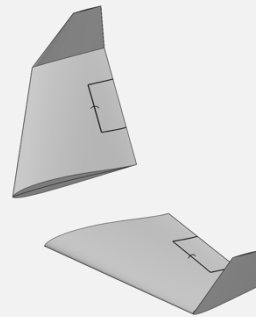


Figure 6. Open VSP Model

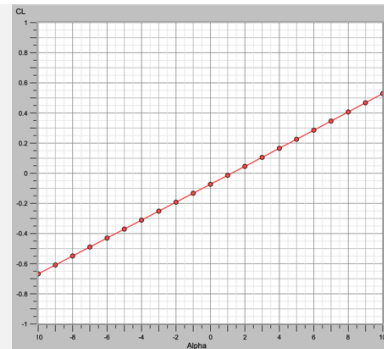


Figure 7. VSP Lift Polar

E. Prototype Development Model

The initial plan for the vehicle was to create a glider weighing 6 pounds which was capable of carrying up to a 2-pound payload. Conceptual design, fabrication, and initial testing were completed for this model. After a month into the project and discussions with AE department faculty, a decision was made to redesign and downscale the project to a 1-2-pound vehicle. The reason for the downscale was to reduce risk for damaging other aircraft in the national airspace system and to people and structures on the ground in the event of an unplanned collision. The initial prototype was not a complete waste, as it allowed us to verify that the CNC wire cutter was capable of producing a swept wing. The prototype vehicle also allowed for verification that the drone used for low altitude testing was capable of lifting the vehicle to an appropriate drop altitude.



Figure 8. Prototype Model

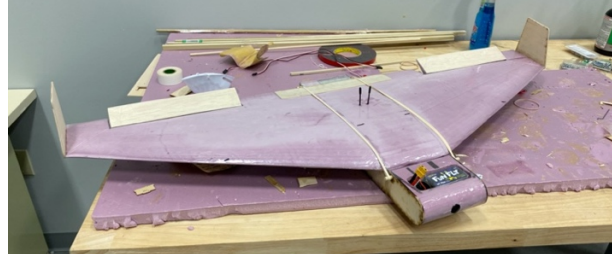


Figure 9. Prototype Model

F. Low Altitude Testing Apparatus



Figure 10. PARS suspended below the octocopter being lifted for a drop test

In order to perform testing of the vehicle at low altitudes a method was needed to lift the plane up several hundred feet above the ground, since the glider has no capability to provide its own thrust. Several options were explored, including the use of a tethered balloon to lift the glider, and a bungee launch system to get the glider in the air and flying. We also had at our disposal access to a large octocopter (Figure 11), which was borrowed from the project innovation hub on campus. The octocopter had plenty of thrust to lift itself and our glider below it, and it is capable of flying a programmed mission to an exact drop altitude. The repeatability and convenience that the octocopter provided over the other two options are why it was selected as the lifting method for low altitude testing. Beneath the octocopter was roughly 20 feet of kite string, which was long enough to allow the glider to be out of the extremely turbulent downwash that the octocopter generated and reduced the spinning that the glider experienced during the ascent. The end of the kite string was attached to the release pin, which slid into the mechanism on the glider and secured the glider until the pin was released and the glider dropped. At the end of the kite string a small weight was also added, which prevented the string from whipping back up and into the rotors of the octocopter after the glider was released (Figure 10).



Figure 11. Octocopter used for testing

selected as the lifting method for low altitude testing. Beneath the octocopter was roughly 20 feet of kite string, which was long enough to allow the glider to be out of the extremely turbulent downwash that the octocopter generated and reduced the spinning that the glider experienced during the ascent. The end of the kite string was attached to the release pin, which slid into the mechanism on the glider and secured the glider until the pin was released and the glider dropped. At the end of the kite string a small weight was also added, which prevented the string from whipping back up and into the rotors of the octocopter after the glider was released (Figure 10).

G. Mission Power Requirements

The estimated total mission time for an ascent and glide back from 100,000 feet is roughly 2 hours. An excel sheet was created in order to account for the power draw requirements of all of the components (Table 2). Servo current was measured and averaged, and the current draw of each of the components was measured. Initially, a 1.5 Amp-Hour 4s LiPo battery was selected to power the vehicle. Which would have provided around 5 hours of power. A larger power safety margin was desired, and so a new battery was assembled from 3 21700 cells, which created a 5 Amp-Hour 3s Lithium Ion battery. This upgrade tripled the

Parameter	Current	Unit	Voltage	Unit	Power	Unit
Pixhawk + GPS	0.28 amp		5 volt		1.4 Watt	
Raspberry Pi Zero	0.12 amp		5 volt		0.6 Watt	
TBS XF Receiver	0.1 amp		5 volt		0.5 Watt	
Servo Average Current	0.2 amp		5 volt		1 Watt	
Camera	0.1 amp		5 volt		0.5 Watt	
GPS Tracker	0.1 amp		5 volt		0.5 Watt	
APRS Transmit	0.46 amp		5 volt			
APRS IDLE	0.005 amp		5 volt			
APRS Transmit Frequency	30 seconds					
APRS Transmit Time	3 seconds					
Average APRS Current	0.0505 amp		5 volt		0.25 Watt	
				Total:	4.75 Watts	
Battery:	5 AH		12 volt		60 Watt Hour	
Avg 5V Current Draw:	0.85 Amp					
Main Battery Run Time:	12.62 Hours					
APRS Backup Battery	0.55 AH		4 volt		2.2 Watt Hour	
APRS Backup Runtime:	8.71 Hours		Total Time:		21.33 Hours	
Crossfire Backup Battery	0.2 AH		4 volt		0.8 Watt Hour	
Crossfire Backup Mode Current	0.02 amp		4 volt		0.08 Watts	
Crossfire Backup Runtime:	10 Hours		Total Time:		22.62 Hours	
GPS Backup Battery	72 Hours		Total Time:		84.62 Hours	

Table 2. Energy requirement estimations

battery power available, while only increasing the battery weight by 10%.

Meeting the power requirement to perform the base mission is the main priority. However, in the event of a malfunction or alternate landing site, power will be needed to power the onboard tracking system for as long as possible in order to increase the chances of vehicle recovery. There are 3 main tracking devices on the vehicle: TBS Crossfire receiver telemetry, an APRS position transmitter, and a GPS tracker. The function of each of these will be discussed in more detail later on. Each of these systems are charged and ran off of the main battery, but also have their own backup power supplies in the event that the main battery dies or is separated during a crash. The TBS Crossfire will switch to a low power mode when main power is lost which simply broadcasts its last known GPS location back to the ground station. The GPS tracker has its own backup battery as well and will continue for roughly 3 days while updating position every 5 minutes. The GPS tracker update rate can be remotely adjusted to a slower timeframe to gain even more run time. The APRS tracker has a mini UPS power switcher which will switch power to a small single cell lipo battery and continue broadcasting location when the main battery dies.

H. Model Construction Methods

1. CNC Hot Wire Cutting Swept Wings

XPS foam was selected as the model build material due to its desirable insulation properties and ease of construction. A CNC hot wire cutter (Figure 12) was used to cut the desired wing size and shape into the XPS foam. The design of our vehicle required a swept wing to be built, which initially was an issue. While the CNC hot wire was physically capable of cutting a swept wing, the current software for the machine only allowed one set of x and y coordinates to be input. This limitation would only allow a straight wing to be cut. To resolve the issue, the code for the machine was rewritten to allow for two sets of x and y coordinates to be specified, one for each of the two gantries. An Excel calculator was created which input the desired root and tip coordinates, chord lengths, twist, sweep, dihedral, and the distance between gantries. The Excel sheet output the two sets of translated and scaled x and y coordinates (Figure 13) which could be input into the updated CNC hot wire software for cutting.

2. CNC Milling Foam Interior

The interior of the body was cut out in specific locations to create pockets for all of the components to be mounted. Some of the gaps between pockets were very tight, and so CNC cutting the holes allowed for a clean finish and for all of the components to have a protected mounting location (Figure 14).



Figure 12. CNC hot wire cutting the XPS foam wing



Figure 13. Excel sheet used to generate the gantry coordinates to be fed to the machine

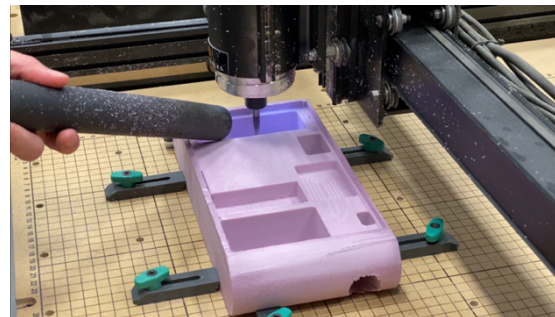


Figure 14. CNC milling the interior slots in the XPS foam body

3. Fiberglass Reinforcement

After completion of CNC wire cutting and milling the XPS foam components to form the main structure of the vehicle, it was announced that access to the on-campus labs would be restricted for the rest of the semester due to the closing of campus. Fortunately, most construction methods could be adapted for constructing the vehicle at home without the need for access to on campus labs. However, in the event that the body or wings were damaged beyond repair, it would not be possible to reconstruct them in the same method in which they were built. While XPS foam is a good model building material, it is not resistant to small nicks and bumps which come with repeated flight testing or hard landings. A method to increase the durability of the vehicle was desired to reduce the probability that the vehicle would be damaged beyond repair even in a hard landing event. It was decided to reinforce the body and wings with a layer of fiberglass and epoxy resin. The fiberglass added around 0.1 pounds to the vehicle weight, which is not preferable but deemed a necessary trade off under the circumstances. Fiberglass reinforcement of the model would not be necessary for a single use flight, but the greatly increased durability of the vehicle has allowed it to withstand landings that it previously could not. Shown in Figure 15 is a fiberglass patch added to the bottom of the vehicle to protect the PDB before being repainted to blend in.

4. Battery Pack Assembly

The main battery pack to power the vehicle was assembled by spot welding (Figure 16) three 21700 lithium ion cells together in series to produce a 0.5 AH 3S (~12 Volt) battery (Figure 17). The custom battery back replaced the store bought 0.15 AH 4S (~16 Volt) lithium polymer battery that the vehicle was originally designed to hold, while still maintaining the same shape and fitting in the same pocket on the vehicle. The 21700 cells have a higher energy density than lithium polymer batteries, and so the upgrade resulted in the energy capacity being tripled without the need to modify the vehicle to hold a larger battery.

5. 3D Printed Drop Release Mechanism and Pin

A mechanism was designed to be able to release the vehicle from the tether suspending it on command. The mount which is fixed to the vehicle (Figure 18) has a slot where an HS85 servo is slotted and secured in place. The pin which is attached to the tether (Figure 19) slots into the mount and the servo actuates a small rod which slides into the pin and secures it in place. When the servo pulls the rod out, the pin disengages, and the vehicle is released. Both the mount and pin were 3D printed out of PLA plastic.



Figure 15. Fiberglass patch being installed over the power distribution board



Figure 16. Spot welding nickel strips onto the 21700 battery backs to connect them



Figure 17. Completed battery pack assembly

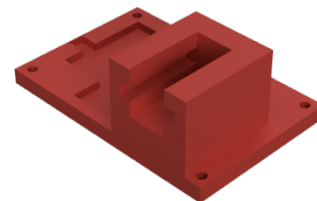


Figure 18. Release mechanism

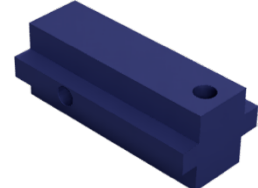


Figure 19. Release pin

I. Final Flight Model

The design of the flight vehicle was determined by utilizing the mission simulation Excel sheet, Open VSP analysis, and by careful component placing in the fuselage to ensure that a desired CG is achieved. The vehicle was modeled in Autodesk Fusion CAD software to aid in component placement and provide the G-Code for CNC cutting. Several aspects of the nature of the mission had to be carefully considered when designing the vehicle. For instance, the two HS-85 servos that control the elevons were placed inside of the fuselage to keep them warm in the extreme cold at high altitudes. The servos actuated the elevons by rotating a torque rod that was connected through the wing to the elevons. The parachute is stored in a tube which slides into the bottom rear of the vehicle, and the two basswood spars which pass through the fuselage had to be carefully positioned to allow them to slide above the parachute tube without interfering with the electronic components. The pitot tube was mounted on the wing and the silicon tubes that run from the pitot tube to the sensor runs through the inside of the wing, this reduces the drag induced by the pitot tube as much as possible. The antennae for the TBS Crossfire receiver are mounted on the winglets, and the antenna for the APRS transmitter protrudes from the rear of the body. The body was painted black to aid in heating the internal components at in the extremely cold environment at high altitudes.

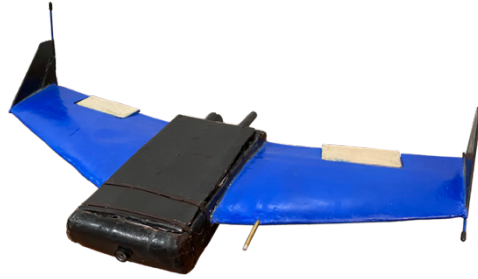


Figure 20. Final Vehicle Assembly

Vehicle Specifications		
Span	25	in
Span per Wing	10	in
Root Airfoil	MH 60	
Root Chord	7.5	in
Tip Airfoil	MH 60	
Tip Chord	4.25	in
Tip Twist	-8	degrees
Tip Dihedral	0	degrees
LE Sweep	25	degrees
Wing Area	0.8	ft^2
Mean Chord	5.875	in
x bar	6.72	in
y bar	4.54	in
CG	5.07	in
Static Margin	28.09%	
Body Length	10	inches
Body Width	5	inches
Body Height	2	inches
Elevon Width	4	inches
Elevon Height	1.5	inches
Elevon Spanwise Start	3	inches
Weight	2	lbf

Table 3. Data sheet of vehicle specifications

Projected Vehicle Performance			
Max Alpha Trim	8	degrees	
Alpha Trim	2	degrees	
Longitudinal Stability	0.38	cm/rad	
Sea Level Stall Speed	45	ft/s	
L/D Max	5		
S/L Cruise Speed at L/D Max	101	ft/s	
S/L Cruise Dynamic Pressure	12.65	psf	
Max Load Factor Before Stall	5.75		
Max Structural Load Factor	10		

Table 4. Data sheet of projected vehicle performance

Item	Weight (lbf)	Arm (from Front) (in)	Moment (lb-in)
APRS Tracker	0.02	7.142	0.14284
Pixhawk	0.079	4.3	0.3397
PDB	0.051	3	0.153
Crossfire Receiver + antennas	0.005	8	0.04
Wing	0.2	10	2
Body	0.15	5.25	0.7875
GPS Tracker	0.079	8	0.632
Camera	0.026	0.5	0.013
Parachute, Tube, and Relay	0.13	12	1.56
Servo Drop Mechanism	0.097	8.5	0.8245
Left elevon servo	0.049	3.77	0.18473
Right Elevon Servo	0.049	3.77	0.18473
Battery	0.61	1.908	1.16388
Raspberry Pi Zero	0.03	6.633	0.19899
GPS 1	0.15	8	1.2
Fiberglass Reinforcement	0.1	5	0.5
Pilot Tube	0.07716	3	0.23148
Adhesive	0.1		
Total Weight:			2 lbf
CG:			5.08 in
Aerodynamic Center:			6.73 in
Static Margin:			28.12%

Table 5. Data sheet of component weight and CG

J. Vehicle Component Overview

1. Pixhawk Mini 4 Autopilot, GPS, and Pitot Tube

The Pixhawk autopilot system is the main brain of the vehicle and it interfaces with the elevon servos to fly the plane based on instructions from the raspberry pi. A Ublox 8MN GPS and external compass feeds the Pixhawk position and heading information, and a pitot tube sends the autopilot total and static pressure measurements. At low altitudes, a pitot tube is not always necessary as the autopilot can get a good idea of airspeed by using groundspeed measurements from the GPS. At higher altitudes there is a much larger discrepancy between indicated airspeed and groundspeed. Since the density of air is greatly reduced at high altitudes, the plane must fly faster in order to achieve the same dynamic pressure. If the autopilot did not compensate for this effect and attempted to only use groundspeed to fly the vehicle, it would think it was flying too fast and attempt to pitch up and potentially stall the vehicle. A pitot tube is necessary in order to allow the autopilot to fly the vehicle at a constant indicated airspeed throughout the entire glide. From our calculations, this indicated airspeed will equate to roughly 12.6 psf of dynamic pressure.

2. TBS Crossfire Diversity Nano Receiver

The TBS Crossfire Receiver is a long range 915 Mhz receiver which allows telemetry and control information to be exchanged between the vehicle and ground station throughout the flight. The system also doubles as a tracking device which can assist with finding the vehicle in the event of a malfunction. Antenna polarization is critical in achieving maximum range for radio devices. Ideally, the ground station antenna and vehicle antenna would have the same polarization. The antennas on the vehicle are dipole antennas and the polarization can be adjusted by positioning the antenna either horizontally or vertically. The ground station antenna is vertically polarized, so to achieve the maximum range the antenna on the vehicle would also need to be vertically polarized. The vehicle spends half of the mission nose down on the ascent, and in level flight on the descent. The receiver is a diversity receiver, meaning that it essentially is two separate receivers which are connected to their own antenna and the receiver with the strongest signal is used. This is useful because it allows us to position one antenna on the left wing tip which will be oriented vertically while the vehicle is nose down during the ascent, and a second antenna on the right wing tip which will be oriented vertically while the vehicle is in level flight on the descent.

3. GPS Tracker

A GPS tracker is installed on the vehicle and has the sole purpose of adding another safety net in recovering the vehicle if an unplanned landing is made.

4. APRS Transmitter

APRS (Automated Packing Reporting System) is a widely used transmission feature which allows packets of information to be exchanged over the 2m frequency band. The APRS system is commonly used by operators of high altitude balloon missions and allows vehicle position, altitude, and other sensor data to be transmitted by the vehicle and received on the ground. An APRS transmitter is installed on the vehicle which will allow real time tracking throughout the mission and aid in locating the vehicle.

5. HS-85mg Servos

The HS-85mg servos are high torque metal gear servos, three of them are used on the vehicle to power both of the elevons as well as actuate the release mechanism.

6. Raspberry Pi Zero

A Raspberry Pi Zero runs a python script which sends commands to the Pixhawk to execute the mission. The Pi tells the Pixhawk when to release the vehicle, where to fly, and when to trigger the parachute. The Pi estimates glide distance by calculating in flight L/D and using wind data collected on the ascent. If the Pi determines that a landing site cannot be reached it has a list of alternate landing sites which it can tell the Pixhawk to fly to instead. If any anomaly occurs during the mission such as loss of GPS signal or vehicle control, the Pi will release the parachute.

K. Manual Vehicle Control Testing

The purpose of the manual control flight tests is to ensure that the plane is flying to its expected performance and that the data logging system built in to the Pixhawk is functioning. The plane's ability to recover from the drop with anticipated load factors will be of particular interest. Additionally, alpha trim with full nose up deflection will be determined. The desired data to be collected throughout the manual control flight tests includes horizontal and vertical velocity from the GPS, airspeed, angle of attack, and inertial accelerations in each axis. Using the analysis obtained in VSP, it can be estimated that L/D max will be approximately 5, cruise dynamic pressure will be 12 psf, cruise CL will be 0.2, and cruise CD will be 0.04. Sea level stall speed is projected to be 45 ft/s, however there will only be enough elevon deflection to slow to 54 ft/s at a max alpha trim of 8 degrees.

L. Automated Vehicle Control Testing

The objective of the automated control flight testing is to observe how the autopilot responds to handling navigation on its own to a target location. The python code on the raspberry pi which is constantly updating projected glide distance and planned landing location will also need to be tested. The raspberry pi program will also need to handle mission anomalies such as early or late balloon release, GPS failure, or pitot ice. The desired results of the automated control testing will be to verify that all automation systems and code are functional and that the vehicle is capable of deploying the parachute in the event of an anomaly. The autopilot will be commanded to fly at a dynamic pressure of 12.7 psf, which is what is predicted will be the desired dynamic pressure at L/D max. The raspberry pi is programmed to deploy the parachute in the event of a mission anomaly such as gps loss, or loss of vehicle control. In the event of pitot tube ice, the raspberry pi is programmed to first attempt to change parameters in the pixhawk which will tell it to attempt to estimate airspeed without the airspeed indicator and only the GPS. If altitude is low enough, airspeed should be close enough to groundspeed for the pixhawk to reliably fly the vehicle. However, if the vehicle is at a higher altitude when pitot failure occurs, there will be a much higher discrepancy between airspeed and groundspeed, there is a possibility of loss of control in which case the parachute would be deployed.

M. Pull-Up Maneuver

It can be observed that during the ascent and descent of the mission, the air density decreases as altitude increases. Due to this change, the glider will be experiencing different load factors based on what altitude it is flying at. To ensure that the glider will be able to continue controllable flight throughout the mission, we took the point at which the glider will experience the maximum load factor and plotted the data. This max load factor was found to be at the bottom of a pull-up maneuver, which can be calculated using knowledge from John Anderson's Fundamentals of Flight textbook [3]. The parameters that were needed for these estimates were the minimum and maximum lift coefficient, glider weight, wing surface area, density, and velocity. The values from these calculations at varying altitudes are shown in Figure 21. From the structural analysis of the glider, we found the critical load factors to be positive and negative 10. These data lines are not shown in Figure 21. The maximum velocity at sea level was estimated using previous projects as examples. This value for us came up to be 100 feet per second. This value is shown by the red, vertical line for reference. From this analysis, it can be observed that even at a maximum velocity of 100 feet per second, the glider would only pull about 3.5 g's at 10,000 feet altitude. With a structural limit of 10 g's, we can safely assume that our glider will be able to complete a full mission, even with the varying altitudes.

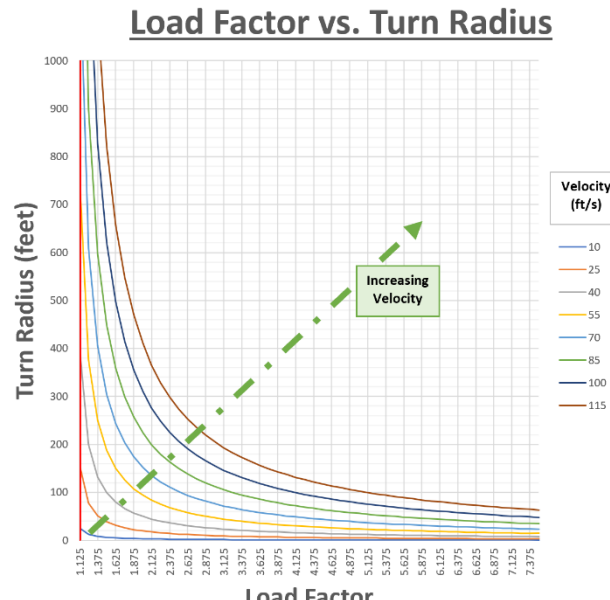


Figure 21. Plot of projected load factors

Turning radius also comes into play when looking at load factors, and the glider's autopilot needs a radius value to coordinate a pull-up maneuver, so we also calculated a radius versus load factor plot to estimate what radii will be safe to pull-up with. Again, using knowledge from John Anderson's text, the turn radius can be calculated using load factor, velocity, and the gravitational constant (32.2 feet per second per second). Simulating this equation at various achievable velocities, we can plot the load factor versus the turn radius required to achieve this load factor. The results are shown in Figure 21.

Even here, at a turn radius of 100 feet, which is tighter than what we would plan on performing, does not produce a critical load factor even at a velocity of 115 feet per second. Note also that the results in Figure 21 do not depend on altitude, so these values are true at any point during the mission.

N. Thermal Testing

At a target altitude of 100,000 feet, temperatures can reach lower than -50 degrees Fahrenheit. This would present issues if the electronics onboard B-PARS were to drop to these temperatures. Most consumer, off-the-shelf components are rated for usage at temperatures above 32 degrees Fahrenheit, so we must ensure that temperatures do not drop below this threshold.

During the predicted mission, it is estimated that the glider will be subjected to these extreme temperatures within the isothermal region of approximately 40,000 feet to 70,000 feet. With reference to standard atmospheric data, this region produces the coldest temperatures at -69.7 degrees Fahrenheit. After this region, the temperature slowly climbs back up to a fiery -51 degrees Fahrenheit. This means that for over half of the ascent and descent, the glider will be in extreme cold. We estimate this time to be approximately 90 minutes of the mission time.

Lucky for us, the glider's body is built from XPS insulation foam, which is meant for keeping warm temperatures in and cold temperatures out. The objective of this thermal test is to predict and observe internal temperatures over the course of 90 minutes in extreme conditions. If the temperatures reach below the 32-degree threshold, the glider can be fixed with more insulation and seals or, if needed, small heating elements powered by the onboard battery.

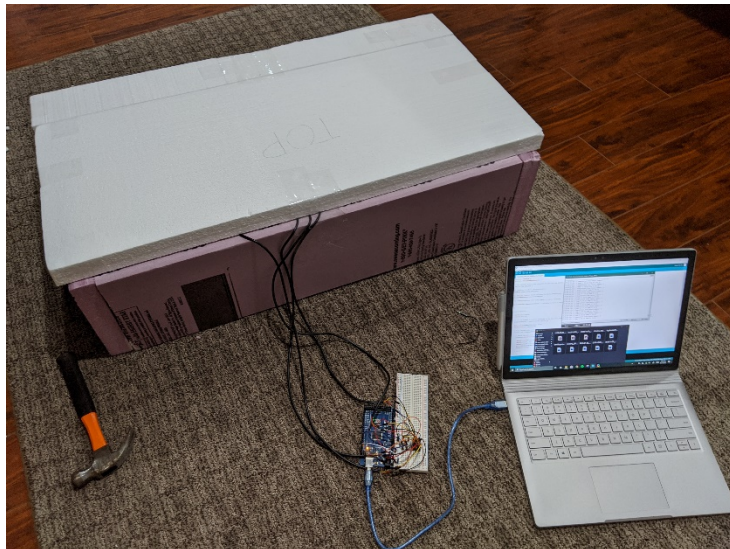


Figure 22. Thermal testing configuration

The test setup starts with the patent-pending foam testing chamber. Made from scraps left over after the glider was made, this testing chamber features highly complex perpendicular corners and removable lid features for easy insertion and retrieval of test articles. The final testing chamber is shown in Figure 22 and Figure 23. Four DS18B20 temperature sensors were connected to an Arduino system which read the temperatures every five seconds. One probe was used to measure the ambient temperature, while the other three were placed inside the glider in the positions described in Figure 24.



Figure 23. Vehicle in thermal testing chamber

The cooling element used was dry ice which sublimates at a temperature of -109.3 degrees Fahrenheit. Though the foam testing chamber possesses a near flawless design, there will not be a perfect seal in the lid which will increase the ambient temperature inside the box from -109 to around -73 degrees Fahrenheit. The interior temperature of the glider will be kept at a comfortable temperature of 70 degrees Fahrenheit and the electronics will be powered on in idle mode to simulate a more accurate thermal test. The extra heat from electronic components was not accounted for when predicted final temperatures inside the glider.

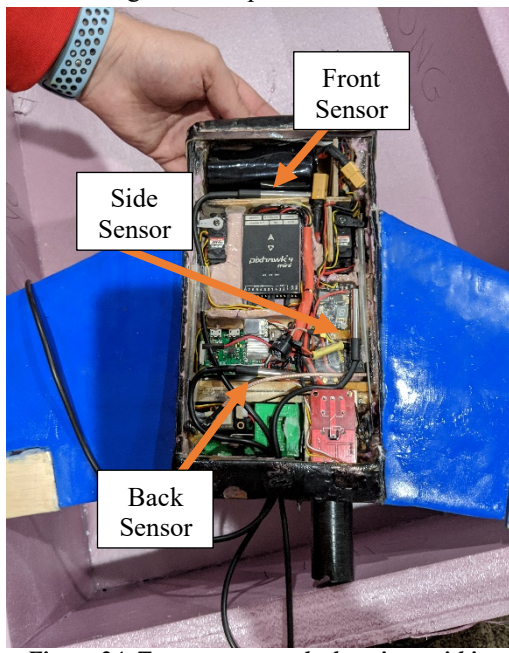


Figure 24. Temperature probe locations within vehicle

Fourier's Law for Heat Conduction can be used here to estimate the final temperatures inside the glider. However, with this method, a couple of assumptions are made that will make the end results vary from the estimated values. First, this method assumes a constant heat transfer rate throughout the entire time. For this thermal test, the heat transfer rate will be constantly changing because the temperatures outside and inside the glider will be changing over time. Second, this assumes that the foam body of the plane and the inside compartment of the glider that it is containing are always at the same temperature. In other words, if the foam decreases in temperature by one degree, it is assumed that the air and electrical components also decrease by one degree. Last, we assume constant thickness of the foam body, even though some parts of the glider are thicker than others.

After computing, it is estimated that the internal temperature of the glider after 45 minutes inside the test chamber will be -5.33 degrees Fahrenheit. The time it will take to reach -30 degrees Fahrenheit

internal temperature will be one hour, and the minimum temperature of the chamber for the internal glider temperature to stay above -30 degrees Fahrenheit will be -269 degrees Fahrenheit. Based on these numbers, it appears that we will need more insulations material or heating elements included in the final design.

O. Parachute Development

The parachute design is largely an adaptation of model rocket parachutes. In a typical model rocket the explosive charge used to launch the parachute out is combined with the engine; a short time after the engine burns out a charge will go off, launching the parachute. Because the plane does not have any sort of engine in it, the "launch charge" had to be designed and made as a separate unit. The entire system is composed of three parts: a modified .223 caliber casing used to hold the Pyrodex (black powder substitute), a relay is used to complete the circuit through nichrome wire to ignite a match and the Pyrodex, and finally the tubular housing used to hold the charge and parachute.

To better fit our needs, the .223 casing had the top third cut off to shorten its length, and the bottom (where the primer originally is) was drilled out to fit the nichrome wire. The wire is put into the bottom and it's plugged with tape, and then the casing is filled with the Pyrodex, and taped over to seal it. This can be seen to the right in Figure 25.

The housing for the parachute was initially designed to fully fit within the body of the plane and was 3D printed to sit flush with the outside edge. Due to shipping delays on the parachute and Coronavirus forcing the plane to be built sooner than intended, the size of the folded parachute had to be estimated. Unfortunately, the estimates made were smaller than the true value and a new tube had to be made. This final one is made from PVC and a wooden cap on the bottom because a 3D printer was not accessible. The final version does stick outside the back of the plane so that the entire parachute can fit, however this is mostly a cosmetic effect. Both the tube, parachute, and final assembly can be seen below in Figures 26 and 27.

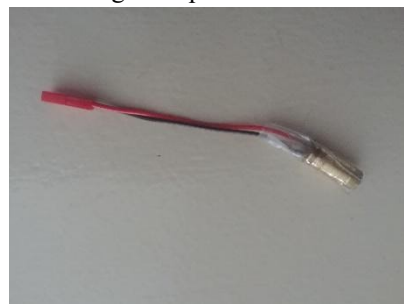


Figure 25. Parachute ejection charge



Figure 26. Parachute and tube



Figure 27. Parachute inserted into tube

III. Results and Discussion

A. Manual Control Vehicle Performance

Manual control flight tests were done at a park near campus with an open field. The tests were carried out by lifting the vehicle to 400 feet above ground level by use of the octocopter. Once the altitude was reached the vehicle was manually released and flown to the ground. The flight path of one of the manual control tests is shown in figure 28, once the vehicle was released it was manually flown in a straight line until landing. Several data points shown in figure 30 were gathered from the flight log where the vehicle was in a steady glide. These data points were reduced to calculate L/D, CL, CD, and dynamic pressure at each of the points. Each of these values were averaged together and displayed in table 6 for the steady glide to obtain an experimental set of flight parameters that the vehicle can be expected to perform at during the gliding descent.



Figure 28. Manual control flight path



Figure 29. Onboard footage from flight test

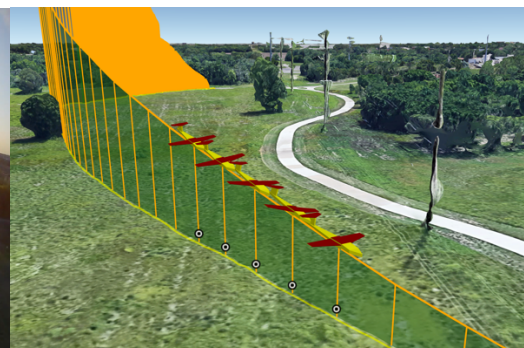


Figure 30. Flight data points used for analysis

The measured values of L/D, CL, CD, and dynamic pressure shown in table 6 closely resemble the engineering estimations obtained prior to testing. The largest discrepancy between predicted and actual flight data is in the predicted airspeed and dynamic pressure. This could be because the vehicle is not matching the 5 degree angle of attack which was predicted to be the location of L/D max. The pixhawk flight log gives an estimation of angle of attack, but the estimation jumps around and does not always seem to be consistent. Because the angle of attack data is not

recorded from an angle of attack sensor, and instead by onboard estimation, it is not fully trusted. L/D, CL, and CD are very close to what the vehicle was expected to perform at.

Manual Control Flight Test Straight and Level Data												
TimeUS	Lat	Lng	Alt (ft)	VX (ft/s)	VZ (ft/s)	Airspeed (ft/s)	L/D	Glide Angle	CL	CD	Q (psf)	AOA (degrees)
910257013	37.737765	-97.30252	1367.03	82.60	20.14	85.02	4.10	13.71	0.30	0.07	8.22	4.43
910436883	37.737739	-97.30257	1363.29	82.63	17.01	84.36	4.86	11.63	0.30	0.06	8.09	1.85
910657036	37.737713	-97.30262	1359.88	82.40	16.98	84.13	4.85	11.65	0.30	0.06	8.05	0.65
910836869	37.737688	-97.30267	1356.53	82.27	15.91	83.79	5.17	10.94	0.31	0.06	7.98	2.79
911036850	37.737663	-97.30271	1353.48	82.47	14.44	83.72	5.71	9.93	0.31	0.05	7.97	3.29
911236923	37.737638	-97.30276	1350.36	81.59	14.21	82.82	5.74	9.88	0.32	0.05	7.80	4.47
Average:			82.33	16.45	83.97	5.07	11.29	0.31	0.06	8.02	2.91	

Table 6. Manual control flight test data points

The measured values recorded in table 7 represent a portion of a manual control flight test where full up elevon deflection was applied to either find stall speed, or alpha max. After full elevon deflection was applied, the vehicle slowed down but did not stall. What was determined was that, as predicted, the elevon deflection on the vehicle was not enough to stall the vehicle. The minimum speed reached and max alpha obtained in the flight test very closely matched the predicted values. Again, the angle of attack estimation is not fully trusted in most circumstances, but it does seem to closely match the expected values in this data set. More inquiry will need to be done to determine how the Pixhawk calculates the angle of attack value that it logs, and in what flight scenarios the angle of attack is most accurate.

Manual Control Full Elevon Deflection Data										
TimeUS	Lat	Lng	Alt (ft)	Elevon Deflection	Airspeed (ft/s)	AOA (degrees)	CL	CD	Q (psf)	
915457134	37.737208	-97.30364	1337.37	Full Nose Up	61.76	5.51	0.57	0.04	4.34	
915656988	37.737192	-97.30368	1336.75	Full Nose Up	60.40	7.88	0.60	0.01	4.15	
915856971	37.737178	-97.30371	1336.75	Full Nose Up	58.61	8.95	0.64	0.03	3.91	
916036838	37.737164	-97.30375	1337.53	Full Nose Up	56.21	8.86	0.69	0.07	3.59	
916256955	37.737152	-97.30378	1338.88	Full Nose Up	54.14	8.93	0.71	0.11	3.33	

Table 7. Full elevon deflection flight test data

B. Automated Control Vehicle Performance

Several automated drop tests were performed where the vehicle autonomously releases itself, recovers from the dive, flies a circle around a target waypoint, and deploys the parachute without any manual input. Figure 32 shows onboard footage from one of these automated tests just before the parachute was deployed, and the flight path is depicted in figure 31. One difficulty in testing automated control from 400 feet low altitude drops is that due to the high glide speed of the vehicle, there is only a 5-10 seconds of flight time before impacting the ground or deploying the parachute. This is not much time to fully test how well the autopilot is circling around the set waypoint because the vehicle gets too low before it can finish an entire circuit. In the tests performed, it was clear that the autopilot was successful in circling the set waypoint. However, higher altitude drops may be desired in the future. Mission anomalies have been tested on the ground by covering the pitot tube, simulating loss of control, and removing the gps to ensure that the raspberry pi will execute the programmed actions. It will be desired to test these anomalies in low altitude drop tests before an untethered drop is attempted.

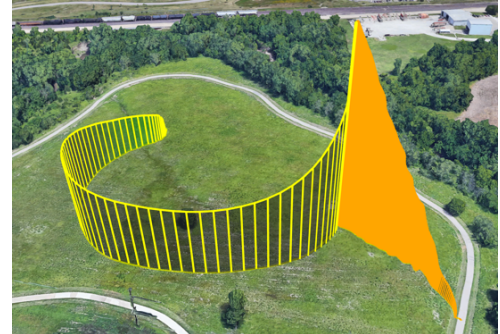


Figure 31. Automated control flight path



Figure 32. Onboard footage from automated control test

C. Flight Testing Difficulties

In order to achieve the desired mission result of the vehicle gliding back to the launch site, our initial analysis concluded that a high wing loading, fast glide speed design was necessary in order to be capable of penetrating strong winds at high altitudes. Several of the difficulties associated with testing a fast glide speed drop from low altitudes were anticipated, such as rough landings, short glide time before reaching the ground, and the need for a large plot of land free of obstructions. What was not anticipated or fully understood was the effect that small protruding features on the vehicle would have on flight performance. This was discovered after two antennae were moved to the exterior of the vehicle.

In early testing, these antennae were kept inside the vehicle as maximum transmission range was not needed for low altitude drops and probability of damage of the antennae were reduced while stored inside of the vehicle body. In anticipation of reaching the final mission configuration of these antennae were moved to the exterior of the vehicle, one protruding vertically from the tail end of the body on the right side, and the other mounted on the top surface of the right wing root. Vertical placement of the transmitter antenna is necessary to achieve maximum range as the polarization of the ground station antenna is also vertical. Previous experience mounting similar antennae on vehicles alluded to the assumption that they would have little effect on flight performance. When the plane was dropped on its first flight after the installation of these antennas, it immediately went into an uncontrollable spiral to the right, there was not enough elevon authority to recover from the spiral and the vehicle crashed into the ground. The cause of the crash was determined to be a combination of placement of both antennae. The antenna mounted on the right wing disturbed the flow over the top surface of the wing, which reduced lift and induced a rolling moment to the right. This effect was intensified by the high wind loading that the wings were already placed under. The antenna mounted vertically on the rear right side of the main body was believed to have caused a nose right yawing moment due to the additional drag produced by the antenna. Both of these effects contributed to a loss of control and crash. The fiberglass reinforcement resulted in no damage to the wings outboard of the root, however the main basswood spars that traverse the body between the wings snapped (Figure 34). This was repaired by doubling both spars through the body section and securing with epoxy. Antenna placement after this incident was considered much more carefully, either by mounting antennae internally or ensuring that placement would not induce a strong enough moment to hinder flight performance.



Figure 33. Flight path of unsuccessful test

surface of the right wing root. Vertical placement of the transmitter antenna is necessary to achieve maximum range as the polarization of the ground station antenna is also vertical. Previous experience mounting similar antennae on vehicles alluded to the assumption that they would have little effect on flight performance. When the plane was dropped on its first flight after the installation of these antennas, it immediately went into an uncontrollable spiral to the right, there was not enough elevon authority to recover from the spiral and the vehicle crashed into the ground. The cause of the crash was determined to be a combination of placement of both antennae. The antenna mounted on the right wing disturbed the flow over the top surface of the wing, which reduced lift and induced a rolling moment to the right. This effect was intensified by the high wind loading that the wings were already placed under. The antenna mounted vertically on the rear right side of the main body was believed to have caused a nose right yawing moment due to the additional drag produced by the antenna. Both of these effects contributed to a loss of control and crash. The fiberglass reinforcement resulted in no damage to the wings outboard of the root, however the main basswood spars that traverse the body between the wings snapped (Figure 34). This was repaired by doubling both spars through the body section and securing with epoxy. Antenna placement after this incident was considered much more carefully, either by mounting antennae internally or ensuring that placement would not induce a strong enough moment to hinder flight performance.

D. Pull-Up Analysis

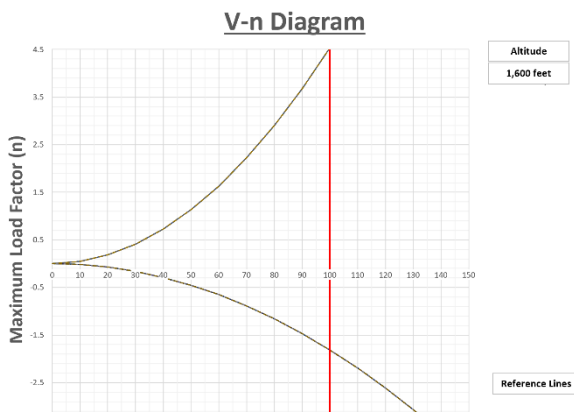


Figure 35. Load factor predictions

Based on our predicted values, at 1,600 feet in altitude, we estimated a maximum load factor of approximately 2.25 at a velocity of 70 feet per second. During the manual pull-up maneuver, this value exactly coincided with the experimentally derived value. During the automated recovery, the load factor pulled was slightly lower than the predicted maximum due to the computer autopilot being able to use a larger turn radius than a manual maneuver. Both times, the load factor was below or at our predicted maximum values, so this data can be trusted for future use. Both load factors were also well below our structural limit of 10 g's.

The predicted values are shown in Figure 35, while the experimentally observed values with trend lines are shown in Figures 36 and 37.

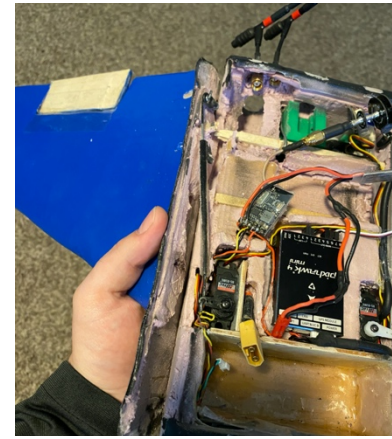


Figure 34. Damaged spar after hard landing

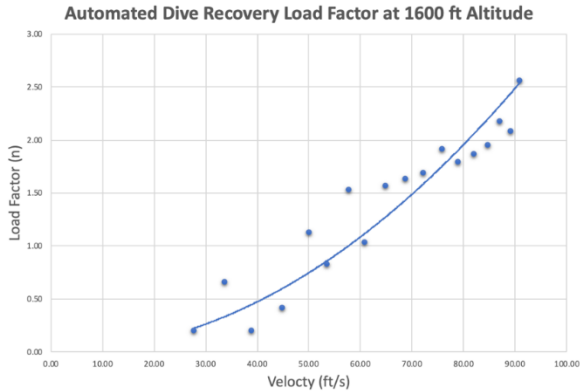


Figure 36. Load factors in automated dive recovery

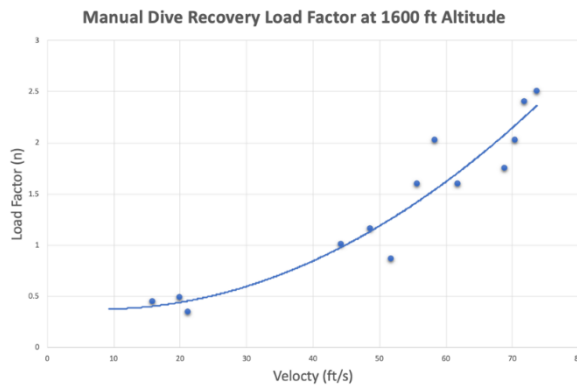


Figure 37. Load factors in manual dive recovery

E. Thermal Testing Results

The results of the thermal testing came out as higher temperatures than expected, which means that we can use our current method of approximating temperature change as a conservative approach to designing a thermally resistive glider. One shortcoming in our testing was using a thermal sensor that could only measure temperatures as low as -55 degrees Celsius, which translates to -67 degrees Fahrenheit. As soon as the sensor reached this threshold, the values would not read correctly, therefore we do not know with 100% confidence what the ambient temperature was inside the testing chamber. We also placed the ambient temperature sensor on the lid of the chamber, which read over 40 degrees Fahrenheit warmer than what the actual temperature was inside the chamber. We still know that dry ice sublimates at -109.3 degrees Fahrenheit, so we can assume that the temperature was somewhere between -109.3 and -67 degrees Fahrenheit, which is plenty cold for our test.



Figure 38. Vehicle just after being removed from thermal chamber

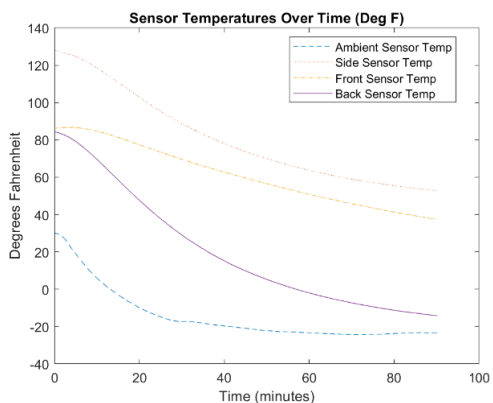


Figure 39. Temperature probe data throughout the test

The glider can be seen in its frosty version after being taken out of the chamber after 90 minutes in Figure 38. The numerical results of the sensors are shown in Figure 39. Observe how different the sensor readings are on the internal values. The heat from the electrical components, as mentioned previously, was not considered when predicting the final temperature values, so therefore we see such a large fluctuation. The side sensor was placed near the video transmitter on the glider which generates the most heat during flight. The final reading after 90 minutes was 52.7 degrees Fahrenheit, well above the 32-degree threshold. The front sensor sat next to the battery

which saw a decent amount of heat, but not as much as the side sensor. The final reading here was 37.4 degrees Fahrenheit. This comes close to the threshold value but survives the test. We will consider adding insulation to this area of the glider. The third sensor placed in the back gave the lowest value after 90 minutes at -23.35 degrees Fahrenheit. This sensor was placed near the orifice in which the probes ran through, which may have skewed this data. We will most likely add a small heating element to this portion to keep the temperatures above the required mark in the future.

The ambient sensor provided reliable values at its location but cannot be trusted as the source for the ambient temperature. A temperature probe able to read values

beyond -67 degrees Fahrenheit is needed for future testing. Another shortcoming of this method was that the box was not chilled to a constant temperature before the glider was inserted. While this method may simulate a slow ascent into colder temperatures, it ultimately avoided our goal of the test of seeing if the electronics reached a certain temperature using a constant temperature thermal chamber. More thermal testing will be necessary to ensure reliable results in the future.

Regardless of these flaws, our electronics were salvaged, and no damage occurred to them despite reaching temperatures below 32 degrees Fahrenheit. This gives us a little more confidence about these components' ability to withstand extreme temperature. A future test may include an automated program to flex the servomotors controlling the elevons to make sure they still operate at below freezing temperatures.

F. Parachute Testing Results

Due to the novelty and possible danger of building a ballistic parachute, several proof of concept experiments were done to ensure the safety and validity of the designs. Additionally, the nature of a parachute system is that testing results are fairly binary: either it works or it doesn't. The effect of the parachute in action can of course be predicted, measured and examined, but the experiments of the system is much less quantitative in nature, and due to limited testing methods.

The initial stationary testing setup involved securing the tube vertically to a post in a team member's backyard (Figure 40). The very first test done only had the charge and protective wadding and was intended to verify the amount of Pyrodex needed to eject the wadding and to ensure the housing could contain the explosion. This test was an overwhelming success. The second test involved adding the parachute to the prior test setup. This was again successful, and the test was successfully repeated two more times to check for consistency.

On the fifth test, the parachute and tube were inserted into the plane to test a horizontal launch from the plane. This test was successful; however, it was discovered that the parachute was being launched with more speed than necessary. The original testing setup had a bird house at the top and it was not realized that in every vertical launch the parachute hit the bird house with a lot of speed, greatly reducing the distance it traveled. After discovering how high the launch force was, the Pyrodex was scaled back by about 50% and testing showed that this was far more appropriate.

Parachute Descent Rate		
Time (s)	Height (ft)	Descent Rate
0.00	51.11	17.60 ft/s
0.29	47.30	20.06 ft/s
0.58	42.91	23.05 ft/s
0.88	37.92	23.26 ft/s
1.17	34.28	17.01 ft/s
1.46	29.62	26.08 ft/s
1.75	24.67	24.13 ft/s
2.04	19.72	25.26 ft/s
2.33	15.19	25.11 ft/s
2.63	9.84	26.51 ft/s
2.92	4.89	22.98 ft/s
3.21	0.00	23.60 ft/s
Mean:		22.89 ft/s

Table 8. Vehicle descent rate after parachute deployment



Figure 40. Parachute static test configuration

The parachute system was then tested on a small drone. The system was secured on it, and the drone was then flown up into the air with the parachute then being successfully deployed. After that, the parachute system was moved onto the actual plane. Many of our flights were landed, with the parachute being an emergency backup, however in the automated flight the parachute was deployed (for the nonemergency reason of testing auto deploy) and the descent rate for the plane can be seen in Table 8. Based on the weight limits and descent rate of the parachute, it was estimated that the plane would fall at around 24 feet per second, and the average experimental descent rate was 22.89 ft/sec, which is reasonably close to the estimate. While this speed is a bit faster than what was initially desired (~17 ft/s), the parachute size was limited by the amount of space in the plane. The plane did experience a 6.5lb force when the parachute deployed, but the parachute is attached to the main spar and this force is well within what the spar is capable of withstanding.

IV. Conclusions

The B-PARS project has allowed for a great deal of learning and experimentation to take place. Several of the construction methods utilized will be very useful to apply to projects in the future. In particular, the capability to cut swept wings out of XPS foam will be very useful to a variety of applications.

The B-PARS project is not yet complete, the designed mission has still yet to be flown. The team plans to acquire more balloons and begin untethered drop testing by increasing the drop altitude for each flight. A few more low altitude drop tests will be desired to verify that mission anomalies can be handled, but there is high confidence in the ability of the vehicle to perform its designed mission.

The main objective of the mission was to have the capability to fly back to the launch location, which required a very fast glider to be able to reliably fly through strong high altitude winds and make the return. If the project were completed again, an alternative landing site may be planned which would allow for the vehicle to fly much slower since it would not need to fight the wind to return to the launch site. A slower vehicle would greatly improve the ease that low altitude drop tests could be performed, and would reduce the probability of damage in a hard landing. In addition, it would reduce the need for a parachute as the vehicle could safely land at slower speeds, therefore removing a good deal of complexity from the vehicle.

Acknowledgments

This project was assisted by Nathan Smith of Wichita State's project innovation hub for providing us with the octocopter and manufacturing assistance as well as Dr. Brandon Buerge for his mentorship throughout the project.

References

¹ M. Laiacker, S. Wlach and M. Schwarzbach, "DLR high altitude balloon launched experimental glider (HABLEG): System design, control, and flight data analysis," 2015 Workshop on Research, Education and Development of Unmanned Aerial Systems (RED-UAS), Cancun, 2015, pp. 360-368 <https://ieeexplore.ieee.org.proxy.wichita.edu/document/7441028>

² Buerge, B., and Terlaje, T., "Development of a High Altitude Payload Platform Under the Low Impact Vehicle Paradigm," *AIAA 3rd "Unmanned Unlimited" Technical Conference, Workshop and Exhibit*, 2004.<https://arc.aiaa.org/doi/10.2514/6.2004-6542>

³ Anderson, J. D., *Introduction to flight*, New York, NY: McGraw-Hill Education, 2016.

⁴ Government, USA, "Title 14 part 101 & 107," Electronic Code of Federal Regulations, https://www.ecfr.gov/cgi-bin/text-idx?c=ecfr&tpl=/ecfrbrowse/Title14/14tab_02.tpl

⁵ How Stuff Works, "How does dry ice work?", <https://science.howstuffworks.com/innovation/science-questions/question264.html>

Appendix

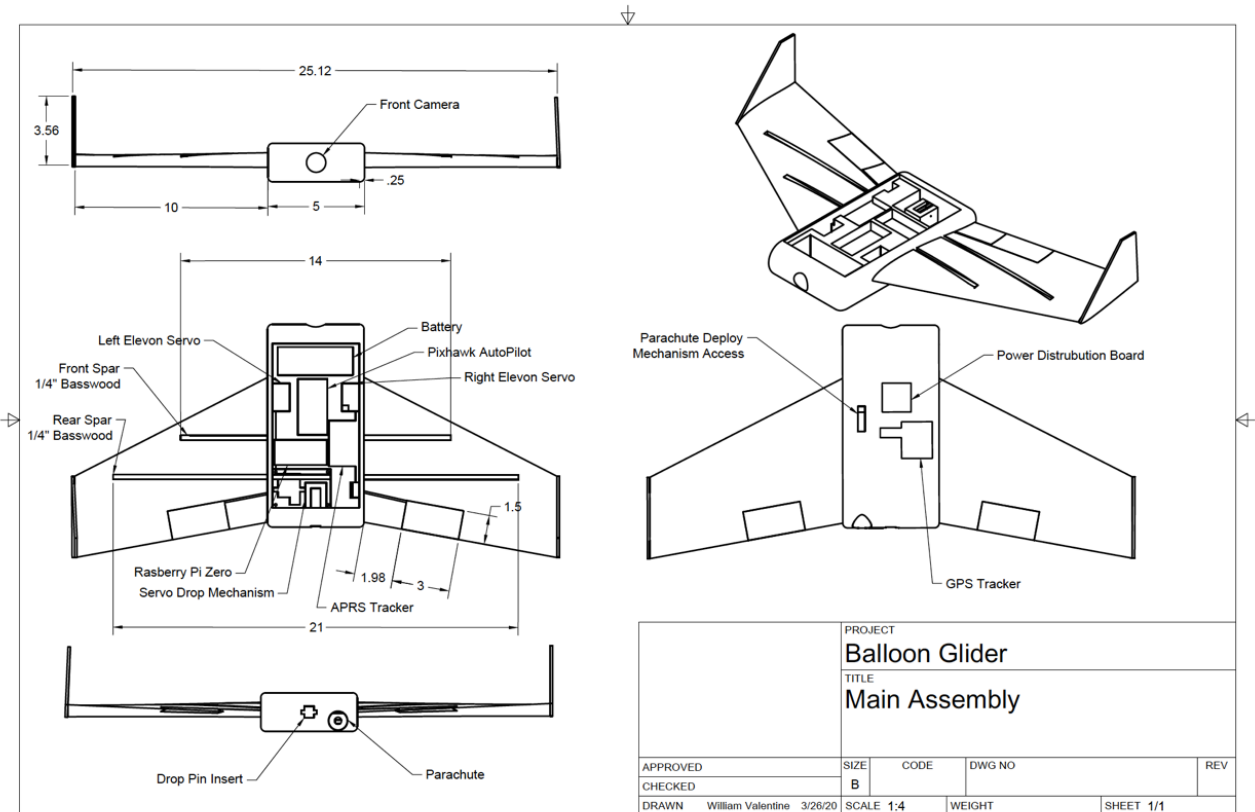


Figure 41. B-PARS Design Drawings



Figure 42. Final Vehicle Assembly before fiberglass reinforcement was added

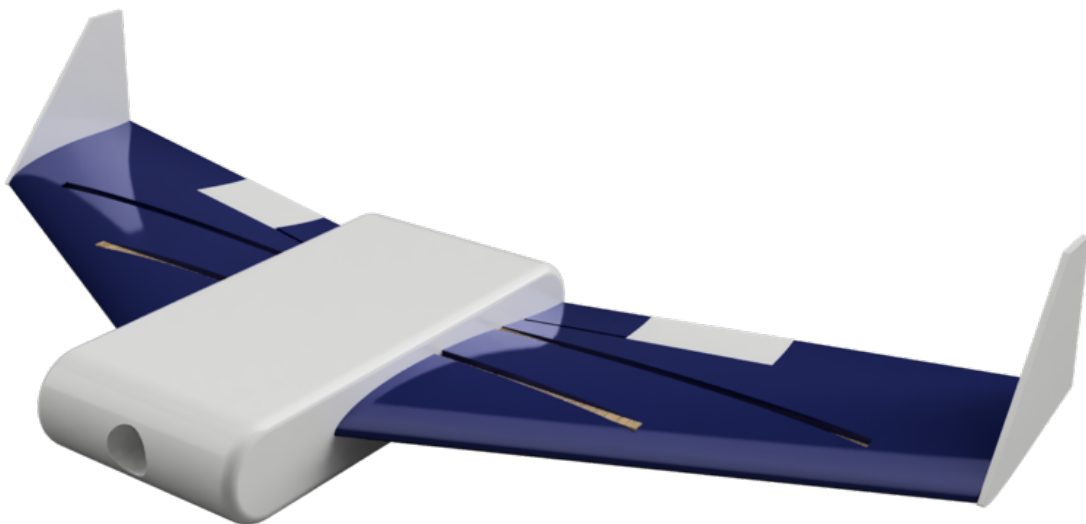


Figure 43. Vehicle CAD Rendering

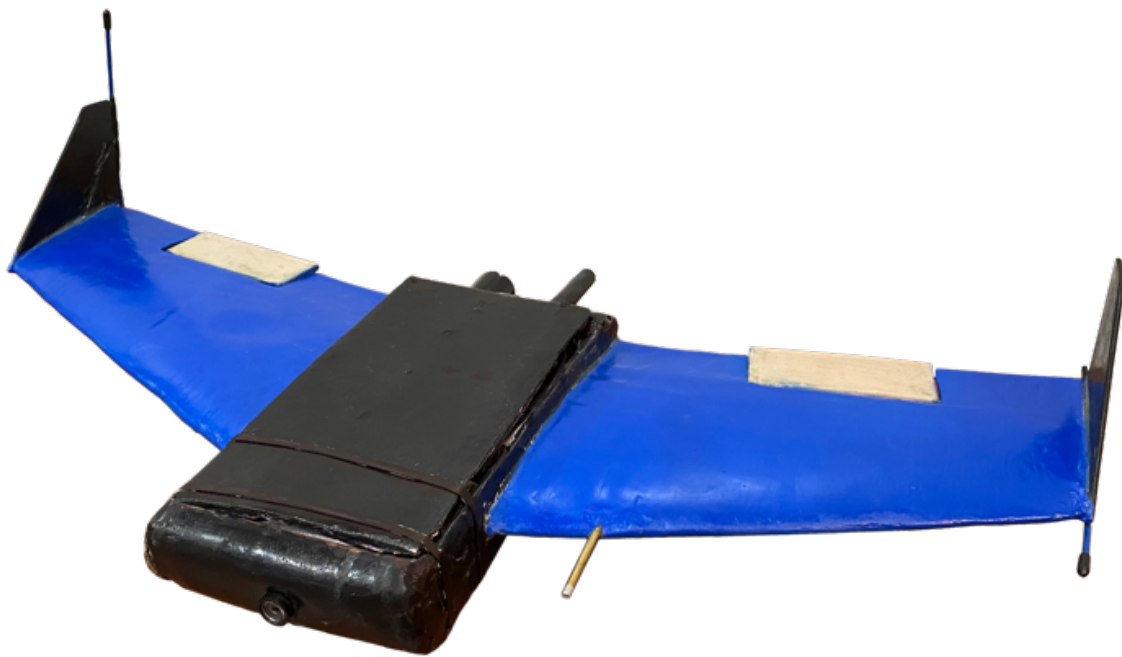


Figure 44. Final vehicle design after fiberglass reinforcement and paint

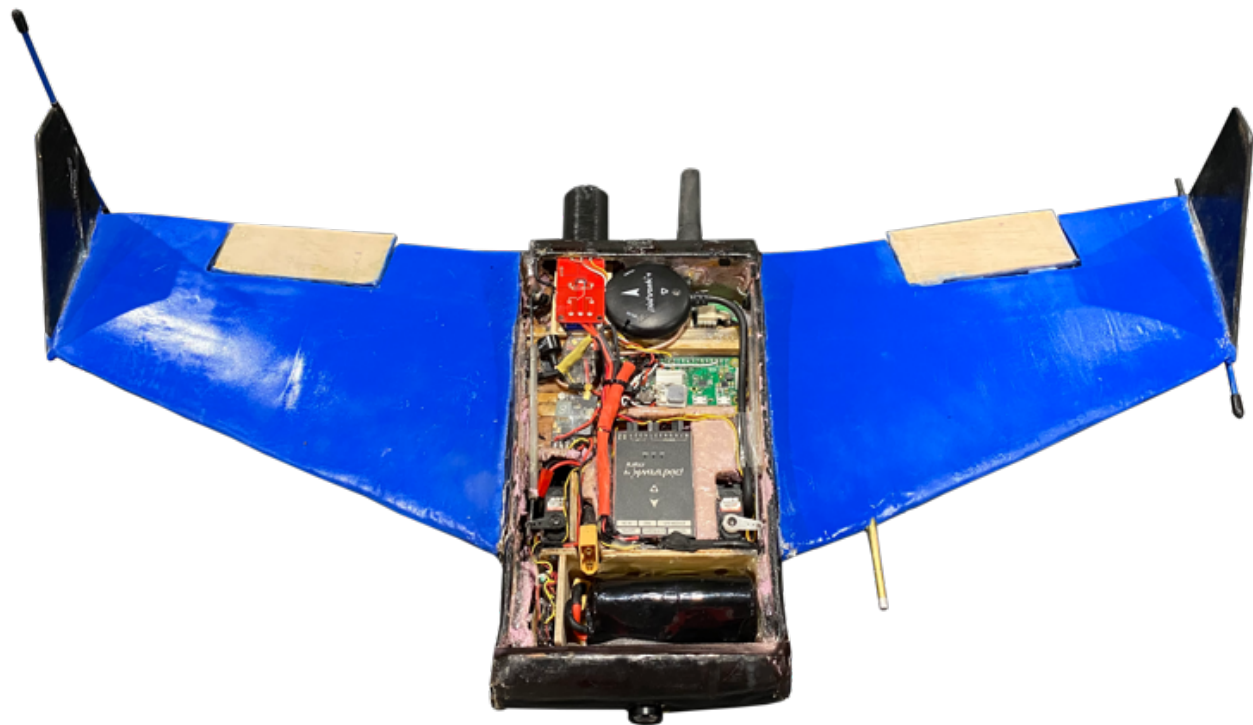


Figure 45. Final vehicle design showing interior layout of components

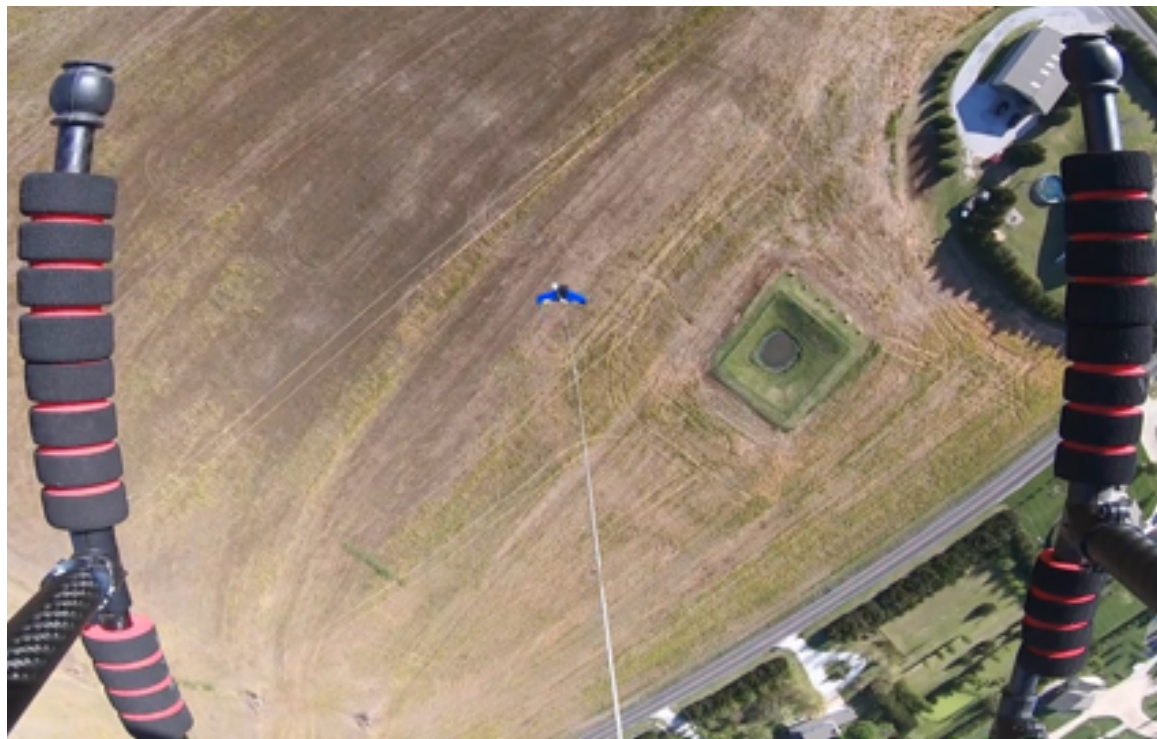


Figure 46. Drop test view looking down from the octocopter at the vehicle just before it drops



Figure 47. B-PARS in flight



Figure 47. Onboard footage from one of the manual control flight tests